Accepted Manuscript

Identifying weakly-interacting single domain states in Ni nanowire arrays by FORC

Mariana P. Proenca, Célia T. Sousa, Joao Ventura, Javier Garcia, Manuel Vazquez, Joao P. Araujo

PII: S0925-8388(16)34269-4

DOI: 10.1016/j.jallcom.2016.12.340

Reference: JALCOM 40263

To appear in: *Journal of Alloys and Compounds*

Received Date: 1 December 2016

Accepted Date: 26 December 2016

Please cite this article as: M.P. Proenca, C.T. Sousa, J. Ventura, J. Garcia, M. Vazquez, J.P. Araujo, Identifying weakly-interacting single domain states in Ni nanowire arrays by FORC, *Journal of Alloys and Compounds* (2017), doi: 10.1016/j.jallcom.2016.12.340.

Identifying weakly-interacting single domain states in Ni nanowire arrays by FORC

Mariana P. Proenca[a,b,*], Célia T. Sousa[a], Joao Ventura[a], Javier Garcia[c], Manuel Vazquez[d], Joao P. Araujo[a]

[a] *IFIMUP and IN - Institute of Nanoscience and Nanotechnology and Dep. Física e Astronomia, Univ. Porto, Rua do Campo Alegre 687, 4169-007 Porto, Portugal*
[b] *Instituto de Sistemas Optoelectrónicos y Microtecnología (ISOM), Universidad Politécnica de Madrid, Avda. Complutense s/n, 28040 Madrid, Spain*
[c] *Institute of Nanostructure and Solid State Physics, Universität Hamburg, Jungiusstraße 11, 20355 Hamburg, Germany*
[d] *Instituto de Ciencia de Materiales de Madrid, CSIC, 28049 Madrid, Spain*

Abstract

The control and understanding of magnetization reversal mechanisms and magnetostatic interactions in nanomagnet arrays is a critical point that has to be overcome in order to reach industrial applications. However, usual magnetic characterization techniques can only provide information on the overall array behaviour and are not able to discriminate relevant local properties. In this work, we show that the first-order reversal curve (FORC) method is a unique tool to identify weakly-interacting uniaxial single domain (SD) particles in systems with complex mixed magnetic states. We compare the FORC diagrams of two sets of Ni nanowire (NW) arrays electrodeposited in hexagonally ordered nanoporous alumina templates: A) with a uniform length distribution (interacting SD particles), and B) with a non-uniform length distribution. For non-uniform length distributions, regions of isolated NWs occur in the array, creating a complex mixture of strongly and weakly-interacting SD particles. These weakly-interacting NWs are here identified by a characteristic ridge along the coercive field axis of the FORC diagram. Micromagnetic simulations confirmed the presence of this weakly-interacting magnetic behaviour in the array with non-uniform length distributions. Combining FORC results with micromagnetic simulations, we show

*corresponding author
Email address: marianapproenca@gmail.com (Mariana P. Proenca)

that the magnetization reversal of interacting wires occurs by the nucleation of transverse domain walls at the NWs' ends, while isolated wires nucleate vortex domain walls. This work thus highlights the importance of the FORC method for the accurate identification and understanding of local magnetic behaviours in nanomagnet arrays.

Keywords:
Magnetic nanowires, FORC, magnetostatic interactions, single domain state, switching field distribution
07.05.Tp, 75.60.Ej, 75.60.Jk, 75.75.-c, 81.07.Gf

1. Introduction

The increased interest in magnetic nanodevices has boosted the recent research on the magnetic properties of nanoelement arrays. In particular, Ni nanowire (NW) arrays are potential candidates for applications in magnetic storage devices, sensors, biomedical chips and magnetically assisted drug carriers [1, 2, 3, 4]. The accurate understanding of the magnetic properties of such NW arrays is thus extremely important for their correct implementation in future devices. In addition, the use of low-cost fabrication techniques, such as Al anodisation [4, 5] and electrochemical deposition [6, 7], has attracted much attention as it further allows the cheap industrialization of such nanomagnet arrays with controlled dimensions.

To study the overall magnetic properties of NW arrays one usually measures the corresponding major magnetic hysteresis loops [$M(H)$] with the magnetic field (H) applied parallel or perpendicular to the NWs long axis [6, 7]. These major $M(H)$ loops allow one to extract important parameters, such as the coercive field, remanence and saturation magnetization of the magnetic array. Nevertheless, the magnetostatic interactions between neighbouring elements, which are known to highly influence the magnetization reversal processes of nanomagnet arrays [8, 9, 10, 11, 12, 13], are not well-described by these major $M(H)$. A simple method to study these interactions is by measuring multiple minor hysteresis loops, the so-called first-order reversal curves (FORCs). This method, proposed by Mayergoyz in 1985 [14], was shown to be quite efficient and powerful in the study of arrays of highly interacting magnetic elements [9, 13, 15, 16, 17, 18, 19, 20, 21, 22, 23, 24, 25, 26, 27, 28]. Each FORC is measured by first saturating the sample at a high positive saturation magnetic field (H_{Sat}), and then measure the magne-

tization by stepping H from a particular reversal field H_r up to a maximum field H_{max} ($H_{max} < H_{Sat}$). The FORC method then consists in measuring a set of FORCs starting at different H_r values that increase in ΔH_r steps ($-H_{max} \leq H_r \leq H_{max}$, $\Delta H_r = H_{max}/50$). These FORCs are then studied through the accurate analysis of the FORC diagram, which is a graphical representation of the FORC distribution $\rho_{FORC}(H, H_r) = -\frac{1}{2}\frac{\partial^2 M(H,H_r)}{\partial H \partial H_r}$, with $H \geq H_r$. To simplify the analysis of the FORC diagram one usually defines the coercive and interaction field axis as $H_c = (H - H_r)/2$ and $H_u = -(H + H_r)/2$, respectively. The quantitative analysis of the ρ_{FORC} profiles along the H_u axis provides information on the magnetostatic interaction fields ΔH_u, measured as the half width at half maximum of the FORC distribution elongation parallel to the H_u axis [10, 25].

Recent works on the study of the magnetostatic interactions in NW and nanotube arrays showed that one can distinguish between local and mean interactions by analysing the ρ_{FORC} profile along the H_u axis [8, 10, 29]. If a distribution narrowly confined around H_c is observed, local magnetic interactions are dominant. However, if the ρ_{FORC} profile is broad along the H_u axis, illustrating a flat top, then mean magnetostatic interactions prevail. On the other hand, weakly-interacting single domain (SD) particles have also been detected by analysing FORC diagrams of complex magnetic systems [20, 30, 31, 32]. These particles were found to have a unique FORC signature that could be used to isolate their contribution from other magnetic components [30]. In particular, the FORC diagram of an array of weakly-interacting SD particles illustrates a narrow ridge along the H_c axis that can be clearly identified even in complex magnetic mixtures [20, 30, 31, 32].

In this work, we use the FORC method to study the magnetic properties of two different Ni NW arrays: (A) with uniform length distributions ($L \sim 9$ μm); and (B) with non-uniform length distributions ($L \sim 3 - 9$ μm). Ni was electrodeposited by pulsed deposition into nanoporous alumina templates with diameters of 35 nm and interpore distances of 105 nm, as described in reference [33], which allowed an accurate control of the NWs' length distribution. A recent study using ferromagnetic resonance showed that the existence of a non-uniform length distribution highly affects the magnetostatic interactions of the array [12]. It is thus highly interesting to further investigate such interaction behaviour using complementary magnetic characterization techniques such as the FORC method. In 2006, Beron *et al.* reported the use of the FORC method to detect the existence of a distribution

of wire lengths in an array of CoFeB NWs with diameters of 175 nm [13]. The analysis of the FORC diagram allowed them to detect two different reversal processes that were ascribed to the existence of two populations of magnetic entities acting differently. However, this model was still under study, and no reports were found afterwards on the detection of weakly-interacting SD states in magnetic NW arrays. Therefore, in this work, we present significant evidence of the use of the FORC method to detect weakly-interacting NWs (that act as SD states) in an array of mixed interacting and weakly-interacting wires. Micromagnetic simulations were also performed using the Object Oriented MicroMagnetic Framework (OOMMF) code from NIST [34], confirming the different switching field distributions of the two sets of NW arrays. Furthermore, using the FORC method we were also able to determine the types of magnetic interactions present in the two different arrays. In particular, for the Ni NWs with inhomogeneous length distributions, a mixture of local and mean magnetic interactions was found. A small ridge along the H_c axis of the FORC diagram was also observed for this array, confirming the existence of weakly-interacting SD states with larger switching field distributions.

2. Experimental details and methods

Hexagonally ordered nanoporous alumina templates were fabricated by a two-step anodisation process of an Al foil (99.997% purity) in 0.3 M oxalic acid at 40 V and 2°C [4, 5]. Prior to the anodisation process, the Al surface was cleaned in acetone and ethanol, and electropolished in a $HClO_4$:C_2H_5OH solution (volume ratio 1:4) at 20 V for 2 min. The first and second anodisations were then performed for 24 and 4 h, respectively, leading to 10 μm-thick alumina templates with highly ordered hexagonal arrays of nanopores (35 nm in diameter and 105 nm of interpore distance).

For the electrodeposition of Ni NWs inside the pores, a pulsed electrodeposition method was employed [6, 33]. The depositions were performed for 1 h in a two-electrode cell with a Pt mesh as the anode and the Al foil as the cathode. The electrolyte used was the so-called Watts bath, composed of 1.14 M $NiSO_4 \cdot 6H_2O$, 0.19 M $NiCl_2 \cdot 6H_2O$ and 0.73 M H_3BO_3, at 40°C. For the deposition current pulse to be applied, the insulating barrier layer present at the bottom of the alumina template was thinned by exponentially decreasing the anodisation voltage, creating dendrites at the bottom of the pores [33]. By tuning the barrier layer thickness (δ_b), one is able to con-

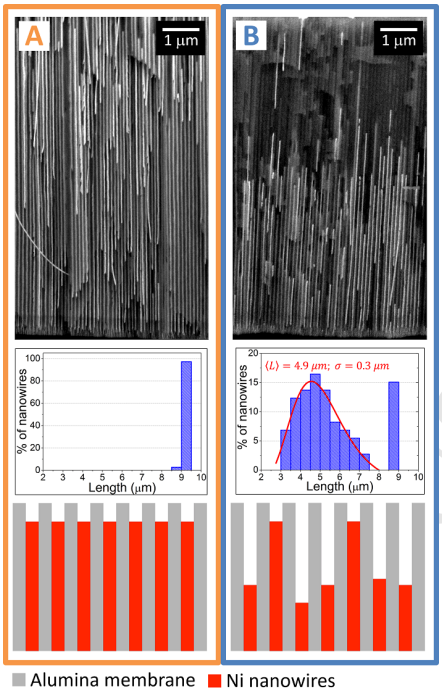

Figure 1: SEM cross-sectional images, histograms of the nanowires' length distribution and schematic representations of the two different Ni NW arrays studied in this work illustrating the uniform (sample A) and non-uniform (sample B) length distributions.

trol the pore filling percentage and length distribution of the subsequently deposited NW arrays, as previously reported [33]. The Ni NW arrays replicated the ordered hexagonal array of pores of the alumina template, having around 35 ± 2 nm in diameter and 103 ± 3 nm of center-to-center distance.

In this work we have analysed in detail the magnetic properties of two extreme cases: (A) Ni NW arrays with homogeneous length distributions ($L \approx 9.0 \pm 0.5$ μm); and (B) Ni NW arrays with a non-uniform length distribution (L between around 3 and 9 μm). The length distributions of the deposited NWs were tuned using different values of δ_b and were evaluated by scanning electron microscopy (SEM, FEI Quanta 400FEG) using the cross-sections of the as-deposited samples. These results were reported in reference [33] for δ_b between 2 and 16 nm, in which the most uniform length distributions were obtained for δ_b between 8 and 12 nm. Figure 1 illustrates the two extreme cases analysed in this work by the FORC method: (A) with

$\delta_b = 9 \pm 1$ nm and (B) with $\delta_b = 2 \pm 1$ nm. The histograms, made by analysing around 70 NWs in each sample, emphasize the uniform length distribution present in sample A (almost 100% of NWs with $L \approx 9$ μm), and the non-uniform length distribution in sample B (only around 15% of NWs have $L \approx 9$ μm and the remaining have an average length of 4.9 μm with a standard deviation of 0.3 μm, estimated by the log-normal fit in Fig. 1).

The Ni NW arrays were magnetically characterized using a vibrating sample magnetometer (VSM, LOT-Oriel EV7) with an applied magnetic field H of up to 15 kOe. To analyse the overall magnetic properties of the array, major $M(H)$ loops were measured with the applied magnetic field parallel and perpendicular to the NWs' long axis. FORC measurements were also performed using VSM, which allowed to extract information on the magnetic interactions and reversal modes of Ni NW arrays with different length distributions.

Micromagnetic simulations were performed using the OOMMF code [34], setting the saturation magnetization value of Ni to 490×10^3 A/m and the stiffness constant to 9×10^{-12} J/m. A parallelepipedic mesh with unit cell size of $4 \times 4 \times 5$ nm^3 along the x-, y- and z-directions, respectively, was used. The stopping condition used in the simulations was $|dm/dt| = 1$ deg/ns with a damping factor of 0.015.

3. Results and Discussion

3.1. Major magnetic hysteresis loops

Figure 2 shows the normalized major magnetic hysteresis loops obtained when applying the magnetic field parallel and perpendicular to the NWs' long axis for both samples. As previously reported in reference [33], independently of the different length distributions of each sample, the $M(H)$ loops evidence an highly anisotropic magnetic behaviour with large squareness (remanence divided by the saturation magnetization) and coercivity values along the parallel direction (easy axis of magnetization) and small squareness and coercivity values along the perpendicular direction (hard axis of magnetization). This is characteristic of single domain-like particles with dominant shape anisotropy, illustrating that the array of magnetic NWs can indeed be considered as an array of SD particles.

Analysing Fig. 2 one can extract the coercivity (H_c) and squareness (S) values for the parallel ($\parallel$) and perpendicular ($\perp$) directions (see Table 1). One can easily observe that the results obtained are similar for both samples,

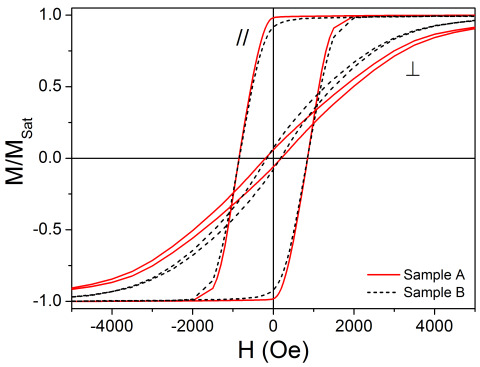

Figure 2: Magnetic hysteresis loops of samples A and B measured with the applied magnetic field parallel (∥) and perpendicular (⊥) to the NW long axis.

with only a slight tilting along the magnetic field axis for the sample with non-uniform length distributions (sample B). Together with the fact that the main parallel coercive field is not sensitively changing in both hysteresis loops, differences in the intrinsic magnetic properties of the nanowires suggest the presence of higher magnetostatic interactions between the NWs (which will be confirmed by micromagnetic simulations and FORC analysis in sections 3.3 and 3.4, respectively). Note also that for sample B a slightly larger susceptibility is detected, seen also as a decrease in the axial anisotropy field ($H_a^{\perp}$) extracted from the perpendicular hysteresis loops (Table 1), which suggests a smaller axial effective anisotropy (likely arising from a reduced effective shape anisotropy [35]). Nevertheless, these results do not allow to fully understand the influence of the different length distributions on the magnetic properties of the array. Therefore, to deepen our study on the magnetic properties of the two different sets of Ni NW arrays, the FORC method was subsequently employed.

3.2. Detecting weakly-interacting SD states by FORC analysis

To further analyse the magnetization reversal processes in Ni NW arrays, FORC measurements were performed with the magnetic field applied parallel to the NWs' long axis. Prior to each FORC measurement the samples were saturated at a high positive magnetic field of $H_{Sat} = 15$ kOe. During each FORC measurement the maximum amplitude of the magnetic field was set to $H_{max} = 2500$ Oe, and the reversal field (H_r) was measured in steps of

Table 1: Coercivity (H_c), squareness (S) and axial anisotropy field ($H_a^{\perp}$) values of the studied samples extracted from the major magnetic hysteresis loops measured along the parallel ($\parallel$) and perpendicular ($\perp$) directions of applied magnetic field.

Sample	$H_c^{\parallel}$ (Oe)	$H_c^{\perp}$ (Oe)	$S^{\parallel}$ (%)	$S^{\perp}$ (%)	$H_a^{\perp}$ (kOe)
A	850±5	195±5	98.1±0.1	5.9±0.1	5.0±0.4
B	850±5	170±10	91.9±0.1	7.5±0.3	3.6±0.4

50 Oe. The FORC distribution was then obtained using a homemade *MatLab* program, in which two auxiliary piecewise cubic spline functions are used to obtain a smoother FORC diagram [19, 36]. Figure 3 shows the FORC diagrams obtained for each sample.

Sample A is made of a uniform array of Ni NWs with similar diameters (35 nm), lengths (9 μm) and center-to-center distances (105 nm). This results in an homogeneous distribution of the magnetization along the array, allowing to express the magnetostatic interaction among the NWs as a net demagnetizing field. This behaviour can be described by the mean field interaction theory (MFIT) in which the interaction field (H_{int}) is proportional to the net magnetization (m), $H_{int} = -\alpha m$, where α denotes the strength of the demagnetizing field at saturation [37, 38, 39]. The FORC distribution of a system which follows the MFIT corresponds to a T-shape, as described elsewhere [9, 17, 27, 29, 40, 41]. The FORC diagram in Fig. 3(a) illustrates a T-shape (evidenced by the black dotted guide line), arising from the magnetic interactions between the nanowires. It is worth mentioning that the distribution observed at larger H_c values does not correspond to real hysterons with such a large coercivity in the system. Coercive values of this ridge towards higher coercive fields correspond to the intrinsic switching field distribution of the magnetically harder nanowires still influenced by the magnetostatic interactions [42]. Since these processes always take place at the end of the overall magnetization reversal, the contribution of the magnetostatic interactions cannot be completely removed by the FORC method, illustrating apparent large coercivity values in the FORC diagram.

Analysing the FORC diagram of Sample B [Fig. 3(b)], one can clearly distinguish the presence of a small elongation along the H_c axis and, more importantly, towards lower values of the coercivity. This effect is similar to the narrow ridges found along the H_c axis of FORC diagrams of mixed

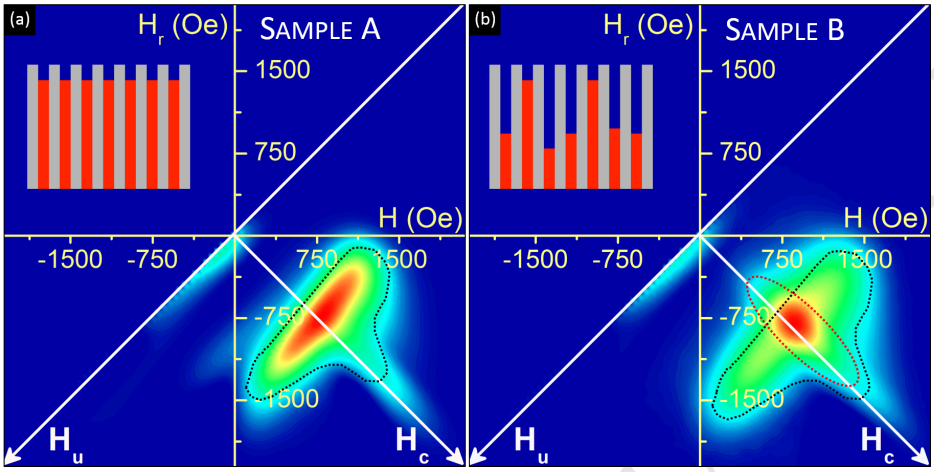

Figure 3: FORC diagrams of samples (a) A and (b) B, when applying the magnetic field parallel to the NWs long axis. The red and black dotted lines are guides to the eye.

complex magnetic systems [30, 31, 32]. These elongations were previously reported as unique signatures of the presence of weakly-interacting SD magnetic particles [30, 32]. Taking into account that the T-shape only shows a ridge towards higher coercivity values from the main distribution, this effect cannot be ascribed to a mere increase of the intrinsic switching field distribution (SFD) because the T-shape should be preserved. The appearance of such distribution towards lower values of coercivity, together with the rhombohedral shape of the most intense peak (red), suggests that two different and, in principle, independent SFDs are present in the system. The FORC diagram can thus be seen as the superposition of two different FORC distributions, as illustrated by the red and black dotted guide lines in Fig. 3(b). The first distribution, similar to that of sample A, arises from the presence of a large number of NWs having the same mean length and therefore showing a T-structure. On the other hand, the NWs whose lengths differ largely from the mean NWs' length, feel a reduction of the magnetostatic interactions since these depend on the distance between the ends of neighbouring NWs where magnetic charges accumulate in ideal magnetic dipoles. In the present case, the length distribution is so pronounced that the NWs with larger length deviation only feel weak interactions, behaving as weakly-interacting SD particles. Furthermore, these NWs with larger differences in their lengths have different switching/coercive fields (also evidenced by mi-

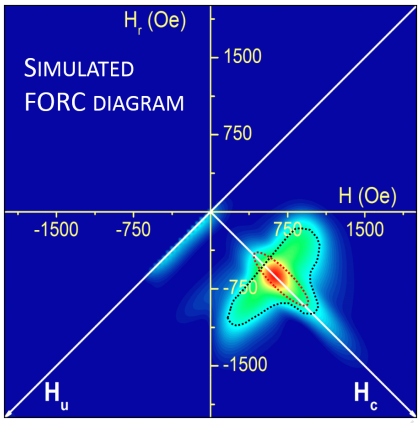

Figure 4: Simulated FORC diagram obtained by combining the experimental FORC data of sample A with a non-interacting switching field distribution, evidencing the presence of two different switching field distributions.

cromagnetic simulations in section 3.3), thus increasing the intrinsic SFD, which will correspond to a FORC distribution elongated along the H_c axis [40, 37, 43].

In Fig. 4, a simulated FORC diagram is represented, in which a superposition of two different FORC distributions have been used: a non-interacting SFD ($\langle H_c \rangle = 821$ Oe; standard deviation $\sigma = 217$ Oe) and the experimental FORC data of sample A. The magnetization curves of the non-interacting SFD were simulated by integration of a normal Gaussian distribution along the magnetic field axis. Then, these magnetization curves were superposed with the experimental ones measured in sample A. Finally, the FORC was evaluated, providing the diagram of the mixed system. The values of $\langle H_c \rangle$ and σ chosen for the non-interacting distribution were those that better fit with the experimental FORC diagram of sample B by direct comparison of the diagrams. After the evaluation of the FORCs, the resultant FORC distribution (Fig. 4) illustrates a similar shape to the experimental one obtained for sample B [Fig. 3(b)], pointing out that the distortion of the FORC distribution along the H_c axis comes from a superposition of the magnetization reversal of weakly-interacting SD nanowires (non-interacting SFD).

To better distinguish between the coercivity distributions of the two samples, cross-sections of the FORC diagrams along the H_c axis are represented in Fig. 5, where a clear broadening of the ρ_{FORC} profile can be observed for

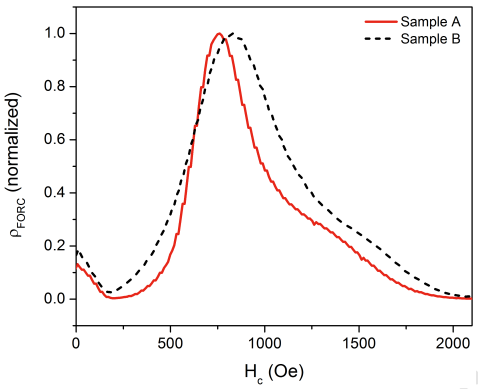

Figure 5: Cross-sections of the FORC diagrams along the H_c axis for the two sets of Ni NW arrays electrodeposited, illustrating the broadening of the coercivity distribution for sample B.

sample B.

3.3. Magnetization reversal: micromagnetic simulations

The magnetization reversal mechanisms of a hexagonal array of Ni NWs with different length distributions were also studied by micromagnetic simulations using the OOMMF code [34]. Seven Ni NWs with 36 nm in diameter disposed in an hexagonal array with 105 nm of center-to-center distance were simulated. The length, L, of the NWs varied between 100 and 200 nm, ensuring aspect ratios higher than 2.5 and avoiding long simulation times. Two sets of simulations were performed: sample A (7 NWs with $L = 200$ nm), and sample B (6 NWs with $L = 100$ nm and a central NW with $L = 200$ nm). Note that, according to the histograms in Fig. 1, the longer NWs are only present in around 15% of the sample, which corresponds to approximately 1 NW out of 7. To better understand the effect of the magnetic interactions and the NW's aspect ratio on the magnetization reversal processes, two individual Ni NWs with 100 and 200 nm in length, respectively, were also simulated. The magnetic field was applied from 10 to -10 kOe along the axis of the NWs (z-direction) and perpendicular to the NWs' long axis (x-direction).

Figure 6 shows the simulated magnetic hysteresis loops obtained between -5 and 5 kOe of applied magnetic field for sample A, sample B and the two individual NWs with different lengths, when applying the magnetic field

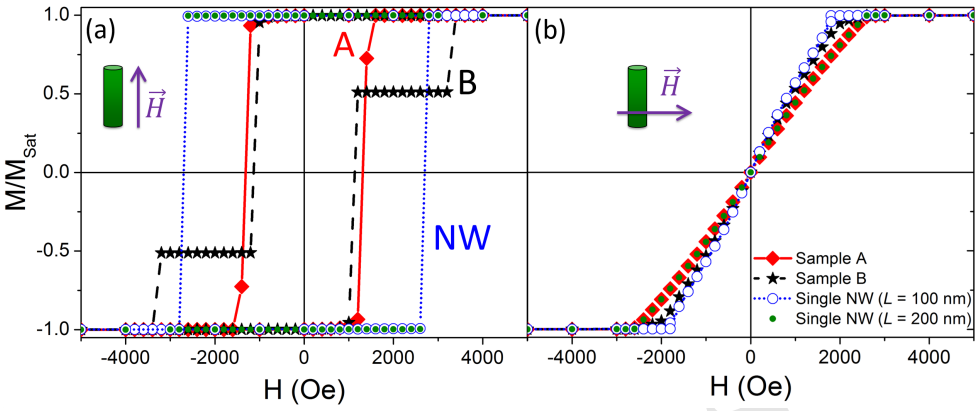

Figure 6: Magnetic hysteresis loops simulated for sample A (red diamonds), sample B (black stars) and a single nanowire with 100 nm (blue open circles) and 200 nm (green filled circles) in length, with the magnetic field applied (a) parallel and (b) perpendicular to the NWs' long axis.

parallel [Fig. 6(a)] and perpendicular [Fig. 6(b)] to the NWs' long axis. Large squareness and coercivity values are obtained along the z-direction (easy magnetization axis parallel to the NWs' long axis), while very low coercivities and squarenesses are obtained when applying the magnetic field along the x-direction (hard magnetization axis perpendicular to the NWs' long axis). As expected, individual NWs have a much higher parallel coercivity (2.4 − 2.8 kOe) than the respective array (1.0−1.4 kOe), as the interactions between neighbouring NWs (in sample A and B) facilitate the nucleation of magnetic domain walls at the NWs' ends, thus reducing the parallel magnetic switching field. When analysing the two individual NWs, the magnetization reversal process along the z-axis is found to be equal for both samples, and thus independent on the NW's length. Nevertheless, a smaller susceptibility was detected for the longer NW [Fig. 6(b)], likely arising from its higher effective shape anisotropy.

The simulated magnetic hysteresis loops for samples A and B also evidence the different switching field distributions obtained when applying the magnetic field parallel to the NWs' long axis. For the 6 NWs located in the outer part of the hexagonal array, the switching field along the z-direction is between 1.0 and 1.4 kOe. However, the central NW exhibits a different magnetic switching field in both studied arrays. For sample A, with NWs of equal lengths, the central NW reverses its magnetization at an applied

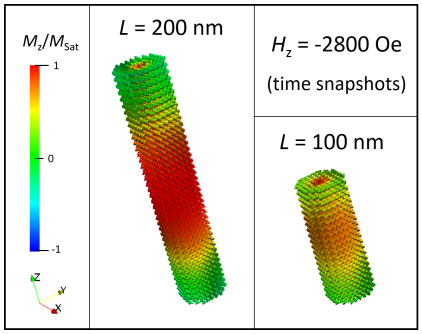

Figure 7: Illustration of the magnetization reversal process in two isolated Ni nanowires with 100 and 200 nm in length, when applying the magnetic field along the z-axis. The colour scale represents the normalized magnetization along the NWs' long axis (z-direction).

magnetic field between 1.4 and 1.6 kOe, which is similar to the switching field of the neighbouring NWs. However, when simulating sample B, with a central NW twice as long as its neighbouring wires, the switching field of the central NW becomes much higher, reaching values between 3.2 and 3.4 kOe.

To better illustrate the magnetization reversal processes of individual Ni NWs and their respective arrays, 3D representations of key equilibrium and time-evolution states were plotted using Paraview [44]. Figure 7 illustrates the magnetization reversal process of the two individual Ni NWs, which occurs at the same applied magnetic field and by the nucleation and propagation of vortex domain walls at the NW's ends. Figure 8 shows the key stages in the magnetization reversal process of samples A and B. For the 6 external NWs, independently of their length, magnetization reversal occurs by the nucleation of transverse magnetic domain walls at the top and bottom ends of the NWs that evolve towards the central part of the NW [Figs. 8(a) and (d)]. The fact that the reversal process starts at the external NWs can be seen as a mere effect of using a low number of NWs in the simulated cell. Therefore, in this case, the lowest energy of the system is most likely achieved by switching the external NWs first, thus blocking the magnetization of the central NW of the cell and avoiding magnetic frustration. Note also that, while moving towards the centre, the nucleated transverse domain walls evidence a combined transverse/vortex character, as also described in references [45, 46, 47]. As for the central NW, it exhibits a different reversal process, depending on the length of the neighbouring wires. In sample A,

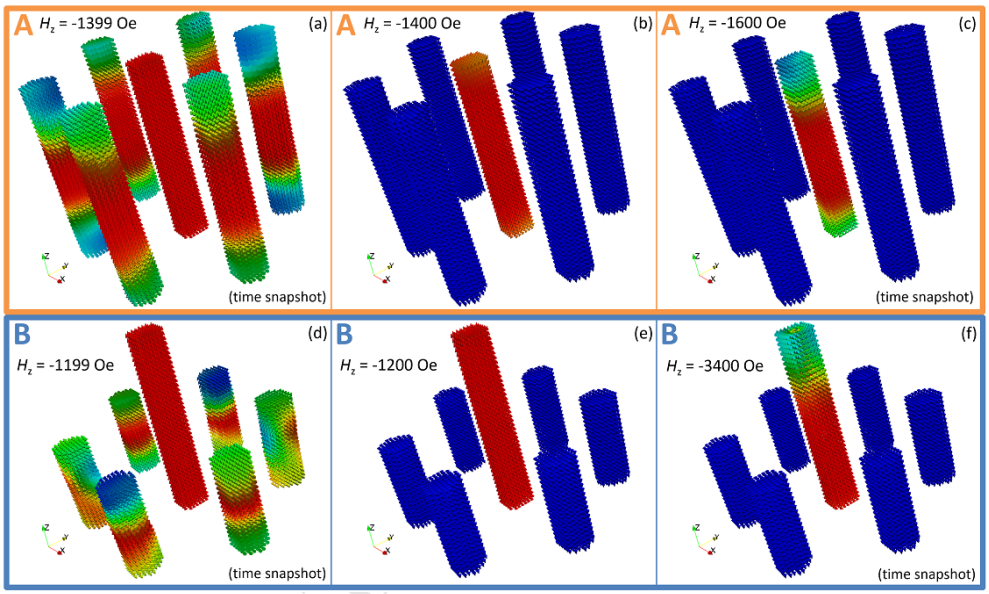

Figure 8: Illustration of the magnetization reversal processes in samples (a, b and c) A and (d, e and f) B, after saturating the nanowires at 10 kOe along the z-axis. The colour scale is the same as the one in Fig. 7.

where all NWs have equal lengths, the central NW reverses its magnetization the same way as its neighbouring NWs, at just a slightly higher applied magnetic field [Fig. 8(c)]. However, in sample B the magnetic moments of the central NW are well stabilized by the antiparallel coupling with the outer NWs [48] [Fig. 8(e)]. In this case, the simulations evidence that the longer central NW (in sample B), not only needs a much higher magnetic field to switch its magnetization, but it does so by nucleating a single vortex domain wall at the top end of the NW [Fig. 8(f)], which then propagates towards the lower end of the wire. These results evidence the non-interacting behaviour of the central longer NW, as its magnetization reverses by nucleating a vortex domain wall, as observed in a single NW, and at the most isolated end of the wire. Micromagnetic simulations thus confirm the presence of a mixture of interacting and weakly-interacting NWs in sample B, as measured and interpreted by the FORC method in the previous section.

Finally, the susceptibility of sample B, measured along the x-axis, was also found to be slightly higher than that of sample A [Fig. 6(b)]. In particular, sample A (composed of 7 NWs with $L = 200$ nm) exhibits the same susceptibility as a single NW with $L = 200$ nm; while sample B (composed of 6 NWs with $L = 100$ nm and only one NW with $L = 200$ nm) presents a susceptibility value similar to the one found in a single NW with $L = 100$ nm. These results are in agreement with the experimental data plotted in Fig. 2, thus confirming the presence of a smaller axial effective anisotropy in sample B due to the reduced effective shape anisotropy of the majority of the NWs.

3.4. Magnetostatic interactions by FORC analysis

A quantitative analysis of the FORC diagrams presented in Fig. 3 was also performed along the H_u axis, providing additional information on the magnetic interactions (ΔH_u) between the Ni NWs in the arrays. Figure 9 shows the ρ_{FORC} profiles parallel to the H_u axis for both samples. According to the moving Preisach model [49, 50], the magnetostatic interactions can be seen as a combination of local and mean interaction fields. When local interactions are dominant, the ρ_{FORC} profile along the H_u axis is characterized by a distribution narrowly confined around H_c. On the other hand, if mean magnetostatic interactions between neighbouring NWs prevail, the ρ_{FORC} profile is broadened along the H_u axis, usually presenting a flattened top [8, 10, 29].

Analysing Fig. 9 one can see that sample A (solid red line) exhibits a broad peak with a flattened top, indicating the presence of major mean mag-

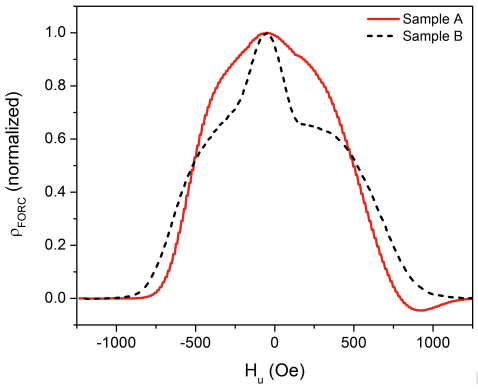

Figure 9: Cross-sections of the FORC diagrams along the H_u axis for the two sets of Ni NW arrays electrodeposited, illustrating the different shapes of the interaction field distributions.

netostatic interactions ($\Delta H_u^A \approx 500 \pm 100$ Oe) between neighbouring NWs. Since all NWs have similar lengths ($L \approx 9.0 \pm 0.5$ μm), and thus constant center-to-center distances (~ 105 nm), the dominance of mean magnetic interactions between adjacent wires was expected. On the other hand, sample B (dashed black line) presents a distribution narrowly confined around H_c with a broad base, emphasizing the presence of a mixture of local and mean magnetostatic interactions between the NWs. As observed in the previous sections, the non-uniform length distribution of the NWs in sample B provides a unique mixture of states. The bottom part of the sample is composed of highly interacting NWs with $L \approx 5 \pm 2$ μm and constant center-to-center distances (~ 105 nm). This part exhibits a mean magnetostatic interaction field between the NWs slightly higher than the one exhibited in sample A ($\Delta H_u^B \approx 640 \pm 100$ Oe), but still very close to ΔH_u^A when considering the measurement error. Note that the field error has been estimated as 100 Oe since a field step of 50 Oe was used and two measurements (H_r and H) performed during the acquisition of the FORCs, thus almost duplicating the field error to around 100 Oe. Moreover, as sample B is the superposition of two different distributions, the H_u profile has to be deconvoluted, and the narrowly confined distribution of the non-interacting phase may result in an overestimation of the interaction field of the interacting distribution within the error. Nevertheless, this minor increase of the mean magnetostatic interactions between the NWs in sample B was also previously observed in

Table 2: Magnetostatic interaction fields (ΔH_u) obtained for the two set of samples using the FORC method.

Sample	ΔH_u (Oe)
A	interacting: 500 ± 100
B	interacting: 640 ± 100
	non-interacting: 110 ± 100

the $M(H)$ measurements as a small decrease in $S^{\parallel}$ (see Fig. 2 and Table 1). These slightly higher interactions may be ascribed to the stronger antiparallel coupling between the shorter and longer NWs, as seen in the micromagnetic simulations. On the other hand, the longer NWs (with $L \approx 9.0 \pm 0.5$ μm) behave as weakly-interacting SD particles. The center-to-center distance between these NWs' top ends is so large, that local magnetostatic interactions prevail. These are identified by the narrowly confined distribution around H_c presented in the ρ_{FORC} profile along the H_u axis (Fig. 9). Note, however, that the non-interacting distribution along the H_c axis has a finite width along the H_u axis due to the measurement resolution and the chosen ΔH_r value [Fig. 3(b)]. As this distribution is not a delta peak it will appear in the H_u profile, giving a strong contribution to the signal around $H_u = 0$. Therefore, the non-interacting field presented in Table 2 should be considered as an approximated value.

The FORC method can thus give us valuable information on the magnetization reversal processes and magnetostatic interactions in nanomagnet arrays, that traditional major magnetic hysteresis loops fail to provide.

4. Conclusions

This work shows how one can use the FORC method to differentiate two types of interactions and switching field distributions in a magnetic array. To achieve that, two kinds of samples have been pre-designed having the same NWs diameters and hexagonal order, but different length homogeneity distributions. Major magnetic hysteresis loops allowed us to conclude that the NWs in the array behave as single domain-like particles dominated by shape anisotropy. However, these measurements were not able to differentiate the magnetic interactions of the different magnetic arrays. Therefore, the FORC method was here used as a way to extract further information

on the magnetostatic interactions present in the array. In sample A, the Ni NWs with uniform length distributions were found to exhibit dominant mean magnetostatic interactions, seen by the broad and flattened peak of the FORC profile along the H_u axis. On the other hand, the Ni NW array with non-uniform length distributions (sample B) presented a mixture of local and mean magnetostatic interactions. These arose from the two sets of NW arrays deposited in sample B: a bottom part composed of interacting NWs with small center-to-center distances (105 nm), and thus higher mean magnetostatic interactions; and an upper part constituted by the isolated longer NWs (average center-to-center distance of NWs' top ends higher than 1 μm), thus exhibiting dominant local magnetic interactions. Micromagnetic simulations confirmed the weakly-interacting behaviour of the longer NWs in sample B. In particular, the magnetization reversal of interacting wires was found to occur by the nucleation of transverse domain walls at the NWs' ends, while isolated wires nucleated vortex domain walls. The analysis of the FORC diagrams also allowed us to state that the Ni NWs with larger length deviations from the array behaved as weakly-interacting single domain particles, as evidenced by the elongation along the H_c axis. This elongation is a unique signature of weakly-interacting SD particles, that can be used to isolate their contribution from other magnetic components. Therefore, the FORC method has proved to be extremely valuable in the identification and study of local and mean magnetic behaviours in nanomagnet arrays.

5. Acknowledgments

MPP and CTS acknowledge FCT for grants SFRH/BPD/84948/2012 and SFRH/BPD/82010/2011, respectively, supported by funding POPH/FSE. JV acknowledges financial support through FSE/POPH and PTDC/CTM-NAN/3146/2014. The authors acknowledge funding from FCT through the Associated Laboratory IN and project UID/NAN/50024/2013, from FEDER and ON2 through project Norte-070124-FEDER-000070, from Spanish MINECO under project MAT2013-48054-C2-1-R and from Comunidad Madrid under project Nanofrontmag S2103/MIT-2850.

6. References

[1] X.-F. Han, S. Shamaila, R. Sharif, Ferromagnetic Nanowires and Nanotubes, in: N. Lupu (Ed.), Electrodeposited Nanowires and Their Applications, INTECH, Croatia, 2010.

[2] X. Kou, X. Fan, R. K. Dumas, Q. Lu, Y. Zhang, H. Zhu, X. Zhang, K. Liu, J. Q. Xiao, Memory effect in magnetic nanowire arrays, Advanced Materials 23 (11) (2011) 1393–1397. doi:10.1002/adma.201003749.

[3] J. H. Tian, J. Hu, F. Zhang, X. Li, J. Shi, J. Liu, Z. Q. Tian, Y. Chen, Fabrication of high density metallic nanowires and nanotubes for cell culture studies, Microelectronic Engineering 88 (8) (2011) 1702–1706. doi:10.1016/j.mee.2010.12.063.

[4] C. T. Sousa, D. C. Leitao, M. P. Proenca, J. Ventura, A. M. Pereira, J. P. Araujo, Nanoporous alumina as templates for multifunctional applications, Applied Physics Reviews 1 (3) (2014) 031102. doi:10.1063/1.4893546.

[5] H. Masuda, K. Fukuda, Ordered Metal Nanohole Arrays Made by a Two-Step Replication of Honeycomb Structures of Anodic Alumina, Science 268 (1995) 1466–1468.

[6] K. Nielsch, F. Muller, A.-P. Li, U. Gosele, Uniform Nickel Deposition into Ordered Alumina Pores by Pulsed Electrodeposition, Advanced Materials 12 (8) (2000) 582–586.

[7] M. P. Proenca, C. T. Sousa, J. Ventura, M. Vazquez, J. P. Araujo, Ni growth inside ordered arrays of alumina nanopores: Enhancing the deposition rate, Electrochimica Acta 72 (2012) 215–221. doi:10.1016/j.electacta.2012.04.036.

[8] M. P. Proenca, C. T. Sousa, J. Escrig, J. Ventura, M. Vazquez, J. P. Araujo, Magnetic interactions and reversal mechanisms in Co nanowire and nanotube arrays, Journal of Applied Physics 113 (9) (2013) 093907. doi:10.1063/1.4794335.

[9] A. Rotaru, J.-H. Lim, D. Lenormand, A. Diaconu, J. B. Wiley, P. Postolache, A. Stancu, L. Spinu, Interactions and reversal-field memory in complex magnetic nanowire arrays, Physical Review B 84 (13) (2011) 134431. doi:10.1103/PhysRevB.84.134431.

[10] M. P. Proenca, J. Ventura, C. T. Sousa, M. Vazquez, J. P. Araujo, Angular first-order reversal curves: an advanced method to extract

magnetization reversal mechanisms and quantify magnetostatic interactions., Journal of Physics: Condensed Matter 26 (11) (2014) 116004. doi:10.1088/0953-8984/26/11/116004.

[11] J. Escrig, R. Lavín, J. L. Palma, J. C. Denardin, D. Altbir, A. Cortés, H. Gómez, Geometry dependence of coercivity in Ni nanowire arrays, Nanotechnology 19 (7) (2008) 075713. doi:10.1088/0957-4484/19/7/075713.

[12] C. T. Sousa, D. C. Leitao, M. P. Proenca, A. Apolinario, A. M. Azevedo, N. A. Sobolev, S. A. Bunyaev, Y. G. Pogorelov, J. Ventura, J. P. Araujo, G. N. Kakazei, Probing the Quality of Ni Filled Nanoporous Alumina Templates by Magnetic Techniques, Journal of Nanoscience and Nanotechnology 12 (9) (2012) 7486–7490. doi:10.1166/jnn.2012.6535.

[13] F. Beron, L. Clime, M. Ciureanu, D. Menard, R. W. Cochrane, A. Yelon, First-Order Reversal Curves Diagrams of Ferromagnetic Soft Nanowire Arrays, IEEE Transactions on Magnetics 42 (10) (2006) 3060–3062. doi:10.1109/TMAG.2006.880147.

[14] I. D. Mayergoyz, Hysteresis models from the mathematical and control theory points of view, Journal of Applied Physics 57 (8) (1985) 3803. doi:10.1063/1.334925.

[15] C. R. Pike, A. P. Roberts, M. J. Dekkers, K. L. Verosub, An investigation of multi-domain hysteresis mechanisms using FORC diagrams, Physics of the Earth and Planetary Interiors 126 (1-2) (2001) 11–25. doi:10.1016/S0031-9201(01)00241-2.

[16] L. Spinu, A. Stancu, C. Radu, F. Li, J. B. Wiley, Method for Magnetic Characterization of Nanowire Structures, IEEE Transactions on Magnetics 40 (4) (2004) 2116–2118.

[17] C. Pike, C. Ross, R. Scalettar, G. Zimanyi, First-order reversal curve diagram analysis of a perpendicular nickel nanopillar array, Physical Review B 71 (13) (2005) 134407. doi:10.1103/PhysRevB.71.134407.

[18] C. Carvallo, A. R. Muxworthy, D. J. Dunlop, First-order reversal curve (FORC) diagrams of magnetic mixtures: Micromagnetic models and measurements, Physics of the Earth and Planetary Interiors 154 (3-4) (2006) 308–322. doi:10.1016/j.pepi.2005.06.017.

[19] F. Béron, L. Clime, M. Ciureanu, D. Ménard, R. W. Cochrane, A. Yelon, Reversible and quasireversible information in first-order reversal curve diagrams, Journal of Applied Physics 101 (9) (2007) 101–103. doi:10.1063/1.2712172.

[20] R. K. Dumas, C. P. Li, I. V. Roshchin, I. K. Schuller, K. Liu, Magnetic fingerprints of sub- 100 nm Fe dots, Physical Review B 75 (13) (2007) 1–5. doi:10.1103/PhysRevB.75.134405.

[21] H. Chiriac, N. Lupu, L. Stoleriu, P. Postolache, A. Stancu, Experimental and micromagnetic first-order reversal curves analysis in NdFeB-based bulk exchange spring-type permanent magnets, Journal of Magnetism and Magnetic Materials 316 (2) (2007) 177–180. doi:10.1016/j.jmmm.2007.02.049.

[22] T. R. F. Peixoto, D. R. Cornejo, Characterizing magnetic interactions in Ni nanowires by FORC analysis, Journal of Magnetism and Magnetic Materials 320 (14) (2008) 279–282.

[23] R. Lavin, J. C. Denardin, J. Escrig, D. Altbir, A. Cortes, H. Gomez, Magnetic Characterization of Nanowire Arrays Using First Order Reversal Curves, IEEE Transactions on Magnetics 44 (11) (2008) 2808–2811. doi:10.1109/TMAG.2008.2001814.

[24] F. Beron, L. P. Carignan, D. Menard, A. Yelon, Magnetic behavior of Ni/Cu multilayer nanowire arrays studied by first-order reversal curve diagrams, IEEE Transactions on Magnetics 44 (11) (2008) 2745–2748. doi:10.1109/TMAG.2008.2002000.

[25] F. Beron, L.-P. Carignan, D. Menard, A. Yelon, Extracting Individual Properties from Global Behaviour: First-order Reversal Curve Method Applied to Magnetic Nanowire Arrays, in: N. Lupu (Ed.), Electrodeposited Nanowires and Their Applications, INTECH, Croatia, 2010.

[26] K. R. Pirota, F. Beron, D. Zanchet, T. C. R. Rocha, D. Navas, J. Torrejon, M. Vazquez, M. Knobel, Magnetic and structural properties of fcc/hcp bi-crystalline multilayer Co nanowire arrays prepared by controlled electroplating, Journal of Applied Physics 109 (8). doi:10.1063/1.3553865.

[27] C.-I. Dobrota, A. Stancu, What does a first-order reversal curve diagram really mean? A study case: Array of ferromagnetic nanowires, Journal of Applied Physics 113 (4) (2013) 043928. doi:10.1063/1.4789613.

[28] M. P. Proenca, K. J. Merazzo, L. G. Vivas, D. C. Leitao, C. T. Sousa, J. Ventura, J. P. Araujo, M. Vazquez, Co nanostructures in ordered templates: comparative FORC analysis., Nanotechnology 24 (47) (2013) 475703. doi:10.1088/0957-4484/24/47/475703.

[29] F. Beron, L. Clime, M. Ciureanu, D. Menard, R. W. Cochrane, A. Yelon, Magnetostatic Interactions and Coercivities of Ferromagnetic Soft Nanowires in Uniform Length Arrays, Journal of Nanoscience and Nanotechnology 8 (6) (2008) 2944–2954. doi:10.1166/jnn.2008.159.

[30] R. Egli, A. P. Chen, M. Winklhofer, K. P. Kodama, C.-S. Horng, Detection of noninteracting single domain particles using first-order reversal curve diagrams, Geochemistry Geophysics Geosystems 11 (1). doi:10.1029/2009GC002916.

[31] A. R. Muxworthy, D. J. Dunlop, First-order reversal curve (FORC) diagrams for pseudo-single-domain magnetites at high temperature, Earth and Planetary Science Letters 203 (2002) 369–382.

[32] A. P. Roberts, D. Heslop, X. Zhao, C. R. Pike, Understanding fine magnetic particle systems through use of first-order reversal curve diagrams, Reviews of Geophysics 52 (2014) 557–602. doi:10.1002/2014RG000462.

[33] C. T. Sousa, D. C. Leitao, M. P. Proenca, A. Apolinario, J. G. Correia, J. Ventura, J. P. Araujo, Tunning pore filling of anodic alumina templates by accurate control of the bottom barrier layer thickness, Nanotechnology 22 (31) (2011) 315602. doi:10.1088/0957-4484/22/31/315602.

[34] M. J. Donahue, D. G. Porter, Oommf user's guide, version 1.0, Interagency Report NISTIR 6376, National Institute of Standards and Technology, Gaithersburg, MD (USA), http://math.nist.gov/oommf/ (Sept 1999).

[35] E. M. Palmero, C. Bran, R. P. Real, C. Magen, M. Vazquez, Structural and Magnetic Characterization of FeCoCu/Cu Multilayer Nanowire Arrays, IEEE Magnetics Letters 5 (2014) 6700304.

[36] F. Béron, Propriétés magnétostatiques de réseaux de nanofils via les courbes de renversement du premier ordre, Ph.D. thesis, Université de Montréal (2008).

[37] J. Garcia, Magnetization processes in transition metal based nanowire arrays, Ph.D. thesis, Universidad de Oviedo (2014).

[38] J. M. Martinez Huerta, J. De La Torre Medina, L. Piraux, A. Encinas, Self consistent measurement and removal of the dipolar interaction field in magnetic particle assemblies and the determination of their intrinsic switching field distribution, Journal of Applied Physics 111 (8) (2012) 083914. doi:10.1063/1.4704397.

[39] H. J. Richter, The transition from longitudinal to perpendicular recording, Journal of Physics D: Applied Physics 40 (9) (2007) R149–R177. doi:10.1088/0022-3727/40/9/R01.

[40] J. Garcia, V. M. Prida, L. G. Vivas, B. Hernando, E. D. Barriga-Castro, R. Mendoza-Resendez, C. Luna, J. Escrig, M. Vazquez, Magnetization reversal dependence on effective magnetic anisotropy in electroplated Co-Cu nanowire arrays, Journal of Materials Chemistry C 3 (18) (2015) 4688–4697. doi:10.1039/C4TC02988G.

[41] C.-I. Dobrota, A. Stancu, Tracking the individual magnetic wires' switchings in ferromagnetic nanowire arrays using the first-order reversal curves (FORC) diagram method, Physica B 457 (2015) 280–286. doi:10.1016/j.physb.2014.10.006.

[42] P. Sergelius, J. G. Fernandez, S. Martens, M. Zocher, T. Böhnert, V. V. Martinez, V. M. de la Prida, D. Görlitz, K. Nielsch, Statistical magnetometry on isolated NiCo nanowires and nanowire arrays: a comparative study, Journal of Physics D: Applied Physics 49 (14) (2016) 145005. doi:10.1088/0022-3727/49/14/145005.

[43] J. Garcia, V. Prida, V. Vega, W. Rosa, R. Caballero-Flores, L. Iglesias, B. Hernando, 2D and 3D ordered arrays of Co magnetic nanowires, Journal of Magnetism and Magnetic Materials 383 (2015) 88–93. doi:10.1016/j.jmmm.2014.10.165.

[44] J. Ahrens, B. Geveci, C. Law, Visualization Handbook, in: C. D. Hansen, J. C. R. (Eds.), ParaView: An End-User Tool for Large

Data Visualization, Elsevier, UK, 2005, Ch. 36, pp. 717–732. doi:10.1016/B978-0-08-100164-6.00024-2.

[45] N. Jamet, S.and Rougemaille, J. C. Toussaint, O. Fruchart, Head-to-head domain walls in one-dimensional nanostructures: An extended phase diagram ranging from strips to cylindrical wires, in: M. Vázquez (Ed.), Magnetic Nano- and Microwires: Design, Synthesis, Properties and Applications, Woodhead Publishing, UK, 2015, Ch. 25, pp. 727–781. doi:10.1016/B978-0-08-100164-6.00025-4.

[46] V. D. Nguyen, O. Fruchart, S. Pizzini, J. Vogel, J.-C. Toussaint, N. Rougemaille, Third type of domain wall in soft magnetic nanostrips, Scientific Reports 5 (2015) 12417.

[47] D. Castilla, M. Maicas, J. L. Prieto, M. P. Proenca, Depinning process of magnetic domain walls in cylindrical nanowires with a chemical constraint, *submitted to Journal of Physics D: Applied Physics*.

[48] M. Susano, M. P. Proenca, S. Moraes, C. T. Sousa, J. P. Araujo, Tuning the magnetic properties of multisegmented Ni/Cu electrodeposited nanowires with controllable Ni lengths, Nanotechnology 27 (2016) 335301.

[49] C. R. Pike, A. P. Roberts, K. L. Verosub, Characterizing interactions in fine magnetic particle systems using first order reversal curves, Journal of Applied Physics 85 (9) (1999) 6660. doi:10.1063/1.370176.

[50] I. D. Mayergoyz, Mathematical Models of Hysteresis and Their Applications, Vol. 103, Elsevier, Amsterdam, 2003.

Highlights:

- Study of Ni nanowire (NW) arrays with uniform and non-uniform length distributions
- First-order-reversal curve (FORC) analysis and micromagnetic simulations are used
- Strongly- from weakly-interactions in a magnetic array are distinguished using FORC
- Distinct magnetization reversal modes for interacting and isolated NWs are obtained